ATLAS NOTE

ATLAS-CONF-2013-044

April 24, 2013

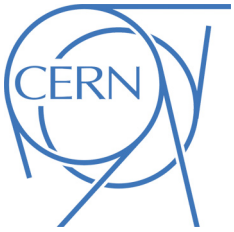

Determination of the tau energy scale and the associated systematic uncertainty in proton-proton collisions at $\sqrt{s} = 8$ TeV with the ATLAS detector at the LHC in 2012

The ATLAS Collaboration

Abstract

This note describes the energy scale calibration of hadronic τ decays and the associated uncertainty in 4.5 fb^{-1}of data at $\sqrt{s} = 8$ TeV recorded in 2012 with the ATLAS detector at the LHC. The calibration is based on simulated τ decays, while the systematic uncertainty is estimated by propagating single particle response measurements to the individual τ decay products, namely charged and neutral pions. The systematic uncertainty on the hadronic τ energy scale for $p_T^\tau > 20$ GeV and $|\eta^\tau| < 2.5$ is found to be $\leq 3\%$ for the hadronic decay modes with exactly one reconstructed track, and $\leq 4\%$ for the hadronic decay modes with at least two reconstructed tracks. The systematic uncertainty is obtained with a deconvolution method, and is checked using an in-situ analysis of the visible mass of reconstructed Z boson decays into one leptonically and one hadronically decaying τ. These two methods yield results that are compatible within the calculated uncertainties.

1 Introduction

Tau leptons play a central role in the LHC physics program, in particular as an important part of the phenomenology of the Higgs boson and Supersymmetry searches [1, 2].

Tau leptons decay hadronically 65% of the time, predominantly to one or three charged pions, a neutrino, and often additional neutral pions. Hadronically decaying τ leptons (τ_h) are categorised by the number of charged decay products, observed as the number of tracks or "prongs". The branching fractions[1] (with respect to all τ decays) for hadronic 1-prongs, 3-prongs, and 5-prongs are approximately 50%, 15%, and 0.1%, respectively. There is also a contribution from Cabibbo-suppressed decays to kaons, with a branching fraction of 3%. For the remainder of this document, $\tau_{\text{1-prong}}$ refers to the hadronic decay modes with exactly one reconstructed track and $\tau_{\text{multi-prong}}$ refers to the hadronic decay modes with at least two reconstructed tracks. Since the hadronic τ decays consist of a specific mix of charged and neutral pions, the energy scale of hadronic τ candidates is derived separately from the jet energy scale. This note describes the calibration of the hadronic τ energy scale (TES) to the energy of the visible decay products, and two methods used to determine the systematic uncertainties on this scale.

First, the TES uncertainty is evaluated by propagating the single particle uncertainties of the individual visible τ decay products ($\tau_{\text{had-vis}}$) to the τ energy scale. These single particle uncertainties are given by an in-situ measurement comparing calorimeter energy measurements to momenta measured in the Inner Detector (E/p) and test-beam measurements (for pseudorapidities $|\eta| < 0.8$), which are used to directly constrain potential differences in the energy response to charged hadrons. For large pseudorapidities ($0.8 < |\eta| < 2.5$), the E/p response measurement for low hadron momenta is combined with uncertainty estimates by comparing different shower models in simulated samples.

Secondly, the uncertainty on the TES is evaluated by using the reconstructed Z visible mass peak from $Z \to \tau\tau \to \mu\nu_\mu\nu_\tau\tau_h\nu_\tau$ events. This provides a cross-check on the systematic uncertainty determined using the former method. The two methods yield consistent results. Both analyses were employed in 2011 data [4]. Because of the denser pileup[2] environment in 2012 data, minor changes were necessary to adapt the earlier methods to the 2012 data-taking conditions as described in Section 2.3 below. The results presented in this note correspond to data and MC samples produced with the software used for reconstruction up to autumn 2012. The in-situ analysis of the visible mass of reconstructed Z boson decays into one leptonically (τ_{lep}) and one hadronically (τ_{had}) decaying τ includes the first 4.5 fb^{-1} of the 2012 data sample at $\sqrt{s} = 8$ TeV.

The note is organised as follows. Section 2 describes the method employed to derive the τ_h energy scale while the deconvolution technique and its application to the TES uncertainty is described in Section 3. Section 4 reports the TES uncertainty derived from the $Z \to \tau\tau$ events.

1.1 Hadronic τ Reconstruction

Decaying τ leptons are reconstructed using the anti-k_t algorithm [5], with a distance parameter $R = 0.4$. Topological clusters[3] [6] made of calorimeter cells, and calibrated using the Local Hadron Calibration (LC) [7] are used as inputs to the jet algorithm. These jets seed the τ_h reconstruction algorithm, which associates tracks to each seed jet. The τ_h reconstruction is applied to all seed jets with $p_T > 10$ GeV and with $|\eta| < 2.5$, the η-range of the ATLAS tracking system.

The LC accounts for the non-compensation of the ATLAS calorimeters, for energy deposited outside the reconstructed clusters, and for dead material. These effects are taken into account using weights applied to the cells. These calibration weights depend directly on the reconstructed shower profile, and

[1] The precise branching ratios used in this analysis are those of the PDG [3].

[2] Pileup in the following refers to the contribution of additional pp collisions superimposed on the hard physics process.

[3] Three dimensional clusters of neighbouring cells for which the signal is significantly above the noise threshold.

are derived from a detailed GEANT4 [8] simulation of the ATLAS detector. The sum of the four-vectors of the clusters associated with the seeding jet is used to calculate the initial direction of the τ_h candidate.

The energy and direction of the reconstructed τ_h at the LC scale are defined by the sum and centroid of all LC clusters within $\Delta R = 0.2$ [4] around the initial jet direction. The mass of τ_h candidates is taken to be zero, and therefore the reconstructed transverse momentum, p_T^τ, and transverse energy, E_T^τ, are identical. The calibration of τ leptons in this note is performed relative to the true visible τ momentum defined in Section 2.1 below.

2 Tau Energy Calibration

The LC improves the τ_h energy resolution with respect to the usage of topological clusters at the EM scale, but does not correct for energy lost before the calorimeters, for underlying event and pileup contributions, and for out-of-cone effects. All of these corrections are needed to restore the true visible τ momentum scale.

The TES is derived from simulated $W \to \tau\nu$, $Z \to \tau\tau$ and $Z' \to \tau\tau$ data samples generated with PYTHIA8 [9]. These samples include in-time and out-of-time pileup[5]. The mean number of reconstructed primary vertices per event is $\langle N_{\mathrm{PV}} \rangle = 14.6$. Events used in this study are selected if there is at least one reconstructed τ_h candidate, and no reconstructed jets with $p_T > 15$ GeV within $\Delta R < 0.5$ of the τ_h candidate. Only reconstructed τ_h candidates passing a medium particle identification criteria, corresponding to a signal efficiency of approximately 60% [10], and matched to a true τ_h with a transverse momentum $p_T^{\tau\text{-true}} > 10$ GeV, are used. Accounting for resolution effects, this calibration is applicable to τ_h candidates with $p_T^\tau > 15$ GeV. Uncertainties are provided for the same transverse momentum range.

This section describes the derivation of calibration constants and corrections that need to be applied to the energy and direction of the reconstructed τ_h to bring it to the true momentum scale and direction. The section follows the order in which the corrections are derived, however they are implemented in the following order: first the pileup offset is subtracted, then the energy is calibrated using response curves and finally an η^τ correction is applied.

2.1 Determination of Calibration Constants

The calibrated momentum p_{cal}^τ is defined as

$$p_{\mathrm{cal}}^\tau = \frac{p_{\mathrm{LC}}^\tau}{R(p_{\mathrm{LC}}^\tau, |\eta_{\mathrm{reco}}^\tau|, n_p)} \tag{1}$$

where R is the additional calibration term determined from simulated events that brings the τ momentum to the calibrated visible momentum scale. It is a function of the reconstructed τ_h momentum at the LC scale p_{LC}^τ, the reconstructed τ_h pseudorapidity $|\eta_{\mathrm{reco}}^\tau|$, and number of prongs n_p (distinguishing one- and multi-prong candidates).

The τ response is defined as the ratio of p_{LC}^τ to the true $\tau_{\text{had-vis}}$ momentum ($p_{\mathrm{vis}}^{\tau\text{-true}}$) and is binned in the true visible momentum and $|\eta_{\mathrm{reco}}^\tau|$. The calibration constants are derived separately for $\tau_{\text{1-prong}}$ and $\tau_{\text{multi-prong}}$ [4]. The τ candidates are grouped into categories by $p_{\mathrm{vis}}^{\tau\text{-true}}$, $|\eta_{reco}^\tau|$ and n_p. In each category, the response is fitted with a Gaussian to determine the mean value and a response distribution is constructed as a function of the mean of p_{LC}^τ in the given $p_{\mathrm{vis}}^{\tau\text{-true}}$ bin. The response is fitted with a functional form empirically-derived and flexible enough to describe the momentum dependence of the calibration constants. The response curves for $\tau_{\text{1-prong}}$ and $\tau_{\text{multi-prong}}$ are shown in Fig. 1(a) and 1(b), respectively. At

[4] $\Delta R = \sqrt{(\Delta\eta)^2 + (\Delta\phi)^2}$.

[5] In-time pileup describing the additional collisions within the same bunch crossing, out-of-time pileup describing the effects due to calorimeter signal tails from collisions in previous bunch crossings.

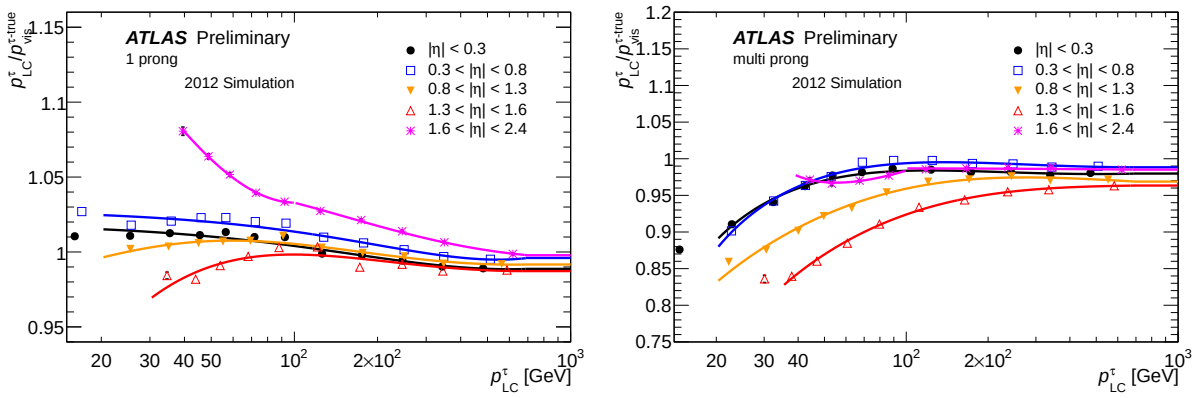

(a) (b)

Figure 1: Response curves as a function of the reconstructed τ_h momentum at LC scale for $\tau_{\text{1-prong}}$ (a) and $\tau_{\text{multi-prong}}$ (b) in bins of $|\eta^{\tau}_{\text{reco}}|$. Uncertainties (smaller than the shown markers in most bins) are statistical only.

very low and high momenta the response curves are extrapolated with a constant equal to the response curve at the outermost evaluated points. The markers terminate at the approximate kinematic limit corresponding to the threshold of $p^{\tau}_{T} = 15$ GeV. The curves extend down to 20 GeV to reflect the fit range used.

2.2 Pseudorapidity Corrections

The calibration procedure described in the previous section brings the momentum of the reconstructed τ_h to the final scale within 1-2% overall. However, a comparison between the reconstructed transverse momentum of τ_h and its true value reveals a few percent level deviation from unity in some $|\eta^{\tau}_{\text{reco}}|$ regions. The largest deviation is found in the transition region between the electromagnetic (EM) barrel and endcap. This is due to clusters reconstructed in poorly instrumented regions of the calorimeters which tend to have underestimated energies, and may lead to a bias in the τ_h pseudorapidity value.

The pseudorapidity of the reconstructed τ_h is corrected to account for this effect. The correction is smaller than 0.01 units in the transition region and negligible elsewhere. The final value of η^{τ} is defined as

$$|\eta^{\tau}| = |\eta^{\tau}_{\text{reco}}| - \eta_{\text{bias}} \tag{2}$$

where $\eta_{\text{bias}} = \langle |\eta^{\tau}_{\text{reco}}| - |\eta^{\tau}_{\text{true}}| \rangle$. After the correction, both the reconstructed momentum and transverse momentum agree with their true values within 1% on average for $\tau_{\text{1-prong}}$ and 2% on average for $\tau_{\text{multi-prong}}$.

2.3 Pileup Corrections

The momentum and pseudorapidity corrections described above restore the response to unity. However, when the response is studied as a function of the pileup conditions, variations of up to 8% are observed. To reduce that dependence and reduce the TES uncertainty, a pileup correction procedure is applied. The pileup contribution to the τ_h momentum is estimated using the following formula

$$p^{\tau}_{\text{pileup}} = A(|\eta^{\tau}_{\text{reco}}|, n_p)(N_{\text{PV}} - \langle N_{\text{PV}} \rangle), \tag{3}$$

where N_{PV} is the number of reconstructed primary vertices in a given event and $\langle N_{\text{PV}} \rangle$ is the mean number of N_{PV} in the sample used to derive the calibration constants ($\langle N_{\text{PV}} \rangle = 14.6$). The parameter A is

extracted in bins of $|\eta^{\tau}_{\text{reco}}|$ and n_p from a linear fit. Given that the fractional pileup contribution is largest for low momentum τ candidates, the offset correction is extracted in a momentum bin corresponding to $20 < p_{\text{vis}}^{\tau\text{-true}} < 30$ GeV for $|\eta^{\tau}_{\text{reco}}| < 1.6$, while for $|\eta^{\tau}_{\text{reco}}| > 1.6$ the momentum bin corresponding to $30 < p_{\text{vis}}^{\tau\text{-true}} < 40$ GeV is used.

Figure 2 shows the pileup contribution per vertex for $\tau_{\text{1-prong}}$ and $\tau_{\text{multi-prong}}$ in bins of $|\eta^{\tau}_{\text{reco}}|$. With pileup corrections applied, equation 1 is modified to

$$p^{\tau}_{\text{F}} = \frac{p^{\tau}_{\text{LC}} - p^{\tau}_{\text{pileup}}}{R(p^{\tau}_{\text{LC}}, |\eta^{\tau}_{\text{reco}}|, n_p)} \tag{4}$$

and defines the τ momentum at final scale after the pileup correction.

The determination of $R(p^{\tau}_{\text{LC}}, |\eta^{\tau}_{\text{reco}}|, n_p)$ is independent of the pileup corrections which adjust p^{τ}_{LC} to the average level of pileup in the samples used to derive the calibration constants. Out-of-time pileup

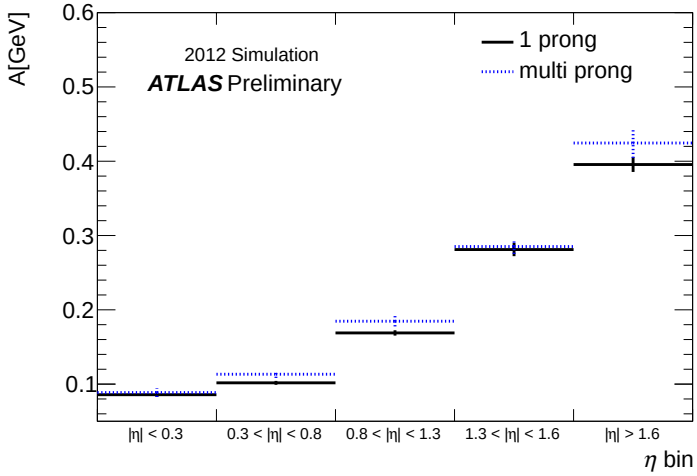

Figure 2: The average pileup contribution per additional primary vertex to $\tau_{\text{1-prong}}$ and $\tau_{\text{multi-prong}}$ in bins of $|\eta^{\tau}_{\text{reco}}|$. The error bars reflect the statistical uncertainty only as extracted from the linear fit.

contributions, originating from previous bunch crossings, are not accounted for. For τ_h with $|\eta^{\tau}_{\text{reco}}| > 2$ and $p^{\tau}_{T} < 20$ GeV, for which the largest pileup contributions are expected, the dependence of the response on out-of-time pileup was found to be less than one percent. These results are based on simulated samples.

2.4 Momentum Resolution

The resolution of the $\tau_{\text{had-vis}}$ momentum is calculated from the difference between the calibrated momentum (p^{τ}_{F}) and $p_{\text{vis}}^{\tau\text{-true}}$. The resolution is obtained from a Gaussian fit by dividing the σ of the Gaussian by the mean value of the $p_{\text{vis}}^{\tau\text{-true}}$. Fig. 3 shows the resolution as a function of the true visible momentum for $\tau_{\text{1-prong}}$ and $\tau_{\text{multi-prong}}$ for $0.8 < |\eta^{\tau}| < 1.3$.

The momentum resolution scales with the momentum approximately as

$$\frac{\sigma}{p} = \frac{a}{\sqrt{p}} \oplus b \tag{5}$$

where $\oplus$ denotes the sum in quadrature. The resolution constants are extracted by fitting this function to the resolution distributions defined above. They are summarised in Table 1 for $\tau_{\text{1-prong}}$ and $\tau_{\text{multi-prong}}$ in various η^{τ} regions.

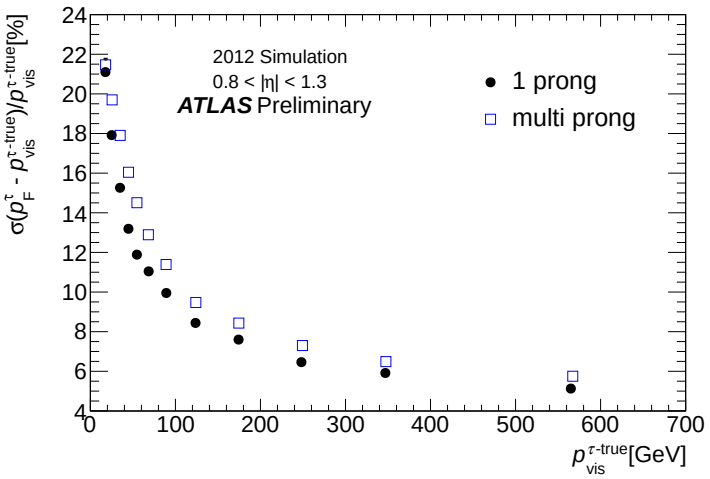

Figure 3: Momentum resolution for $\tau_{\text{1-prong}}$ and $\tau_{\text{multi-prong}}$ for $0.8 < |\eta^\tau| < 1.3$.

The discontinuity in the value of b at $\eta^\tau = 1.6$ is due to a change in the detector technology of the hadronic calorimeter between the barrel and end-cap region. In general, the momentum resolution of $\tau_{\text{1-prong}}$ is about $10 - 20\%$ smaller than for $\tau_{\text{multi-prong}}$ due to the higher fraction of EM energy from π^0 decays relative to the hadronic depositions.

One-prong	$\lvert\eta^\tau\rvert < 0.3$	$0.3 < \lvert\eta^\tau\rvert < 0.8$	$0.8 < \lvert\eta^\tau\rvert < 1.3$	$1.3 < \lvert\eta^\tau\rvert < 1.6$	$\lvert\eta^\tau\rvert > 1.6$
a [$\sqrt{\text{GeV}}$]	0.71	0.73	0.87	1.09	1.10
b	0.02	0.02	0.04	0.07	0.01
Multi-prong	$\lvert\eta^\tau\rvert < 0.3$	$0.3 < \lvert\eta^\tau\rvert < 0.8$	$0.8 < \lvert\eta^\tau\rvert < 1.3$	$1.3 < \lvert\eta^\tau\rvert < 1.6$	$\lvert\eta^\tau\rvert > 1.6$
a [$\sqrt{\text{GeV}}$]	0.85	0.79	1.02	1.24	1.27
b	0.01	0.03	0.04	0.06	0.01

Table 1: Summary of fitted momentum resolution terms for $\tau_{\text{1-prong}}$ and $\tau_{\text{multi-prong}}$ in various $|\eta^\tau|$ bins.

3 Determination of the Tau Energy Scale Uncertainty Using Single Particle Uncertainties

The TES uncertainty has contributions from the calorimeter energy response, the chosen MC event generator with a specific choice of the underlying event model, the detector description in the simulation and systematic uncertainties related to the non-closure of the calibration method. Single particle response measurements can be used to determine the calorimeter response uncertainty by decomposing the τ_h into its decay products and convolving the constituents' response with the $\tau_{\text{had-vis}}$ particle composition. The response of the calorimeter to single particles is estimated from one of three sources depending on the particle kinematics.

1. For low momentum charged hadrons ($p < 20$ GeV for $|\eta| < 1.7$ and $p < 60$ GeV for $1.7 < |\eta| < 2.5$), the response is estimated from in-situ E/p measurements as described in Section 3.1.2.

2. For high momentum charged hadrons in the central region ($|\eta| < 0.8$), the response is estimated from combined test-beam (CTB) measurements [11], as described in Section 3.1.3.

3. In the case of high momentum particles outside the central region, the response is estimated by MC simulation [12] as described in Section 3.1.6.

Sources 1 and 2 directly constrain the description of the calorimeter response to single particles in the simulation and therefore can greatly decrease the TES uncertainty. The convolution is done using a pseudo-experiment approach. In each pseudo-experiment, the TES is evaluated after randomly changing the single particle energy responses within their statistical and systematic uncertainties. In this section, the foundation for the TES uncertainty evaluation is described.

The deconvolution method employed was used and established in the context of the Jet Energy Scale (JES) uncertainty determination for 2010 data [13, 14, 15], as well as in the evaluation of the TES uncertainty for 2011 data [4]. The evaluation of the calorimeter response uncertainty in this document follows the prescription in the documentation cited above while utilising E/p results from 2012 data.

The calorimeter response uncertainty at the LC scale is evaluated as described in Section 3.1; the remaining uncertainty contributions are summarised in Section 3.2. Section 3.3 reports the total TES uncertainty.

3.1 Calorimeter Response Uncertainty

The calorimeter response uncertainty is derived using simulated MC samples of $Z \to \tau\tau$ and $Z' \to \tau\tau$ decays generated with PYTHIA8 [9]. The events are simulated not including additional pileup interactions to allow a pure calorimeter response uncertainty evaluation. The calorimeter response uncertainty is evaluated both for $\tau_{\text{1-prong}}$ and $\tau_{\text{multi-prong}}$ with $p_T^\tau > 15$ GeV. Only reconstructed τ_h candidates passing medium boosted decision tree based particle identification criteria [10] and matched to a true τ_h are used.

The ATLAS simulation software [16] is able to link the simulated energy depositions to the initiating particle in the generated collision. Thus, the in-situ single particle response measurements can be applied to the depositions (given the deposition-particle link) contributing to the reconstructed τ_h candidate. This constrains the uncertainty due to the modelling of the particle-calorimeter interactions and the knowledge of the amount of material in front of the calorimeter. Each particle contributing to clusters associated with the reconstructed τ_h is classified as follows:

- Low momentum charged hadrons. The energy depositions of particles associated with isolated tracks in the Inner Detector are used to determine the energy response $\langle E/p \rangle$ of charged hadrons in a momentum range of $2 \leq p < 20$ GeV for pseudorapidities covered by the tracking system, $|\eta| < 2.5$. This analysis provides a MC to data response ratio.

- High momentum charged hadrons. The pion response measurements of the 2004 CTB data are used to complement the in-situ $\langle E/p \rangle$ measurement for high momentum particles. In the test setup, a full slice of the ATLAS detector, corresponding to the $|\eta^\tau| < 0.8$ region, was exposed to a pion beam with momentum between 20 GeV and 350 GeV.

- Neutral pions. The EM energy response has been studied in detail using electrons from Z boson decays and minimum ionising muons in the hadronic Tile calorimeter. Therefore the EM scale is considered to be well described in the simulation. The uncertainties associated with the EM scale are taken from Ref. [17] and are propagated to the TES.

Figure 4 shows the fractional energy contributions, to $\tau_{\text{had-vis}}$, of particles being classified in one of these three categories for $|\eta^\tau| < 0.3$. For low p_T^τ, the energy scale uncertainty determination is driven by the in-situ $\langle E/p \rangle$ measurement, while the test-beam analysis contributes mainly to the evaluation of the uncertainty at high momenta. The energy contribution from neutral pions does not depend on the $\tau_{\text{had-vis}}$ transverse momentum. The fraction of energy carried by charged hadrons is of the order of 60% for $\tau_{\text{1-prong}}$ and of the order of 85% for $\tau_{\text{multi-prong}}$.

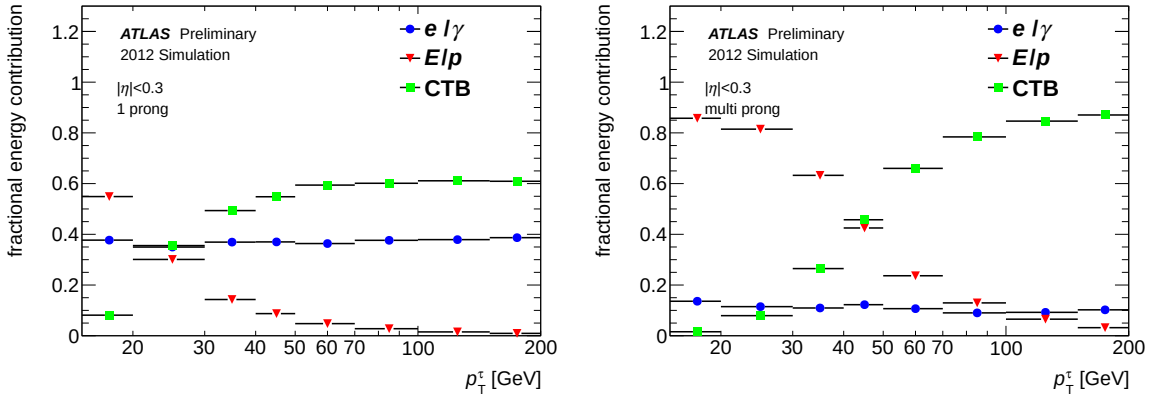

(a) (b)

Figure 4: Fractional energy contributions to $\tau_{\text{1-prong}}$ (a) and $\tau_{\text{multi-prong}}$ (b) for $|\eta^\tau| < 0.3$ by particles described by the $\langle E/p \rangle$ (low momentum charged hadrons), the test-beam analysis (high momentum charged hadrons) and e/γ response measurements (π^0).

3.1.1 Particle Deconvolution

A pseudo-experiment approach is used to propagate the single particle uncertainties to the reconstructed $\tau_{\text{had-vis}}$ [4, 14]. For each pseudo-experiment (t), particle type, momentum (i) and pseudorapidity bin (j) a random factor f_t is sampled from a Gaussian probability density function (PDF) with a mean given by the measured response ratio r between data and MC and its width given by the statistical uncertainties $\Delta r^{(i,j)}$:

$$f_t^{(i,j)} = \mathrm{N}(r^{(i,j)}, \Delta r^{(i,j)}) \tag{6}$$

Systematic uncertainties (δ) of the measurements are included as additional scale factors $u_{t,\delta}^{(i,j)}$, which are sampled from Gaussian PDF's centered at unity and their widths given by the corresponding systematic uncertainty, which themselves may depend on particle type, momentum and pseudorapidity. In each pseudo-experiment t, the $\tau_{\text{had-vis}}$ energy is re-calculated by summing up all energy contributions E_k of the τ object constituents after rescaling them by the corresponding scale factors, giving

$$E_t^\tau = \sum_k (f_t^{(i_k,j_k)} \cdot \prod_\delta u_{t,\delta}^{(i_k,j_k)}) \cdot E_k \tag{7}$$

This energy is compared to the energy as obtained by setting all scale factors $f_t^{(i,j)}$,$u_{t,\delta}^{(i,j)}$ to unity, to assess the TES shift in a given $\tau_{\text{had-vis}}$ object and toy experiment. The mean value $\mu_t = \langle E_t^\tau / E^\tau \rangle$ within the $\tau_{\text{had-vis}}$ sample gives the relative TES shift in the given pseudo-experiment t for a specific set of energy scales and deviations of systematic parameters from one. The distribution of means for a set of 1000 pseudo-experiments is fitted with a Gaussian. The mean of this Gaussian gives information about the expected scale shift between data and MC, while the standard deviation gives the TES uncertainty. Short reviews of the single particle response measurements used as input to the deconvolution method are presented in the following subsections.

3.1.2 Low Momentum Charged Hadrons

The mean energy response for low momentum charged hadrons is measured by comparing their calorimeter energy depositions to the momentum measured by the Inner Detector ($\langle E/p \rangle$). This analysis is performed using a sample of particles with isolated tracks. The neutral background contribution is subtracted

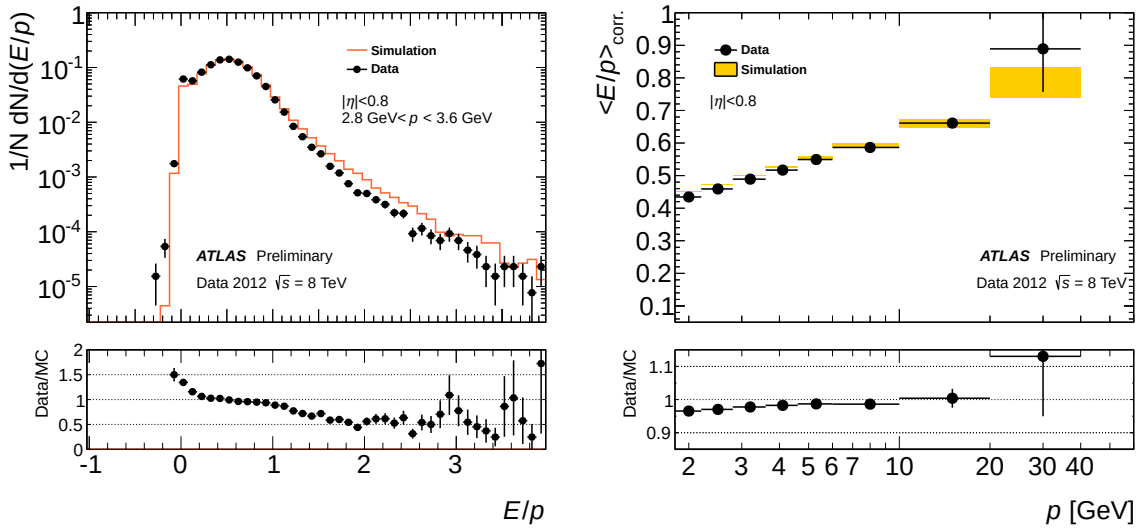

(a) (b)

Figure 5: E/p distribution for track candidates with momenta between $2.8 < p < 3.6$ GeV (a) and the background subtracted $\langle E/p \rangle$ distribution as a function of the track momentum (b). The yellow band corresponds to the statistical uncertainty on the simulated sample.

on average by estimating the average energy density of the calorimeter depositions of neutral particles close to the selected tracks in a sample of late showering, minimum ionising hadrons. This procedure is detailed in Refs. [13, 14, 18]. The comparison of the mean energy response $\langle E/p \rangle$ between data and MC is used to determine a relative response shift in the simulation. This measurement covers momenta up to 20 GeV for $|\eta| < 1.7$ and up to 60 GeV for $1.7 < |\eta| < 2.5$.

In 2012, a dedicated low pileup run at a centre of mass energy of $\sqrt{s} = 8$ TeV was carried out, providing a sample of minimum bias events at a high rate. The average number of interactions per bunch crossing in this run corresponds to 0.01. Figure 5 (a) shows the E/p distribution for particles with momenta between $2.8 < p < 3.6$ GeV. Both the low and the high end tail in the uncorrected E/p distributions are not well modelled in the simulation. The low end tail is dominated by negative energy contributions from cells in the Liquid Argon calorimeter and therefore highly sensitive to energy depositions from previous bunch crossings. Even though the average number of interactions per bunch crossing is low in the studied data sample, contributions from neighbouring bunch crossings still affect this low end tail. The high end tail corresponding to $E/p > 1$ is dominated by energy depositions from neutral particles close to the selected charged track. While these background components are fairly well modelled in 900 GeV data [18], significant deviations from the MC predictions were observed in 7 and 8 TeV data. A background subtraction scheme corrects on average for these neutral depositions. After correction, the mean calorimeter response is well described by MC simulation, with deviations up to 4% at low momenta. Figure 5 (b) shows the background corrected $\langle E/p \rangle$ distribution.

The average energy deposition from pileup interactions is taken into account as an additional noise term in the topological clustering algorithm during event reconstruction. To ensure that the obtained results are applicable to τ_h in nominal 2012 data taking and reconstruction conditions, the impact of the cluster noise suppression on the $\langle E/p \rangle$ analysis was evaluated. Comparisons between different cluster threshold settings as well as comparisons between cell based and cluster based $\langle E/p \rangle$ measurements were carried out. Both comparisons yield compatible results within 2% of the nominal measurement for pseudorapidities of $|\eta| < 1.5$. Therefore a 2% systematic uncertainty is assigned to energy depositions within

this region. For larger pseudorapidities, falling into the acceptance of the hadronic end-cap calorimeter, larger deviations are observed, ranging from 10% for track momenta of 2 GeV to 2% for momenta of 8 GeV.

Additional systematic uncertainties account for the background subtraction scheme (1%), and for differences in the E/p acceptance (<1.5%) [13].

3.1.3 High Momentum Charged Hadrons

The CTB data are used to constrain the calorimeter response for high momentum charged pions [11]. To account for any changes in the calorimeter simulation and calibration method since the CTB data analysis, single charged pions with energies and pseudorapidities corresponding to the test-beam setup are simulated using the current ATLAS simulation setup. The difference in the charged pion response between the two simulations is found to be within 0.5%. In addition, cluster threshold effects are found to be negligible for charged pions with $p > 15$ GeV. Therefore the test-beam results are included in the response uncertainty determination with a conservative 0.5% systematic uncertainty to cover possible response changes in the simulation. Other systematic uncertainties are included to account for the fact that the data are not taken in the same detector conditions. These include uncertainties for calorimeter non-uniformity for all energies measured at the same pseudorapidity point, as well as fully correlated scale uncertainties in the Liquid Argon and Tile calorimeters [14].

3.1.4 Global Electromagnetic Energy Scale

The EM energy scale is precisely measured from the well known line-shape of $Z \rightarrow e^+e^-$ decays for the EM calorimeters and using the energy loss of minimum ionising muons in the hadronic Tile calorimeter. For the EM barrel calorimeter, a 1.5% uncertainty on the cell energy measurement is found, while a scale uncertainty of 3% is found for the hadronic Tile calorimeter. Absolute scale uncertainties are applied to EM energy depositions, such as photons from neutral pion decays, as well as to any particle not falling into the phase space covered by the in-situ $\langle E/p \rangle$ analysis.

3.1.5 Additional Uncertainty Due to Shower Shape Modelling

Differences in the shower shape model can lead to differences in the shower's energy density, and hence to a difference in which cells are included by the clustering algorithm. In the construction of the pseudo-experiments, any effect on the response due to the clustering algorithm is neglected, as only clustered cells are included in the rescaling procedure. The impact of the response uncertainty on the clustering algorithm is studied by re-applying the clustering algorithm after changing the various energy scales in each pseudo-experiment. This effect is found to be negligible, as is the effect of variations in the shower model on the clustering algorithm.

However, changing the distribution of energy in a cluster also changes the LC weight assigned to that cluster, and the τ_h energy reconstruction is based on cluster energies calibrated to the LC scale. The additional uncertainty introduced by this effect is evaluated by comparing the nominal hadronic shower model QGSP_BERT [19, 20, 21] to the FTFP_BERT [22] shower model. Both hadronic shower models, FTFP_BERT and QGSP_BERT, are compared to CTB data. It is found that the full difference between these models gives a realistic scale of the systematic uncertainties associated with the hadronic shower shapes needed for the LC calibration. The effective calibration weight $\langle E_{LC}/E_{EM} \rangle$ is derived by comparing the sum of cluster energies at LC and EM scale and is shown in Figure 6. For $\tau_{\text{multi-prong}}$, deviations of less than 1% are observed between the two physics lists, while for $\tau_{\text{1-prong}}$ deviations are smaller than 0.5%. Similarly, deviations up to 1% are found in the average number of clusters classified as being likely to be of hadronic origin. Alternatively, one can study the double ratio of data to MC comparisons

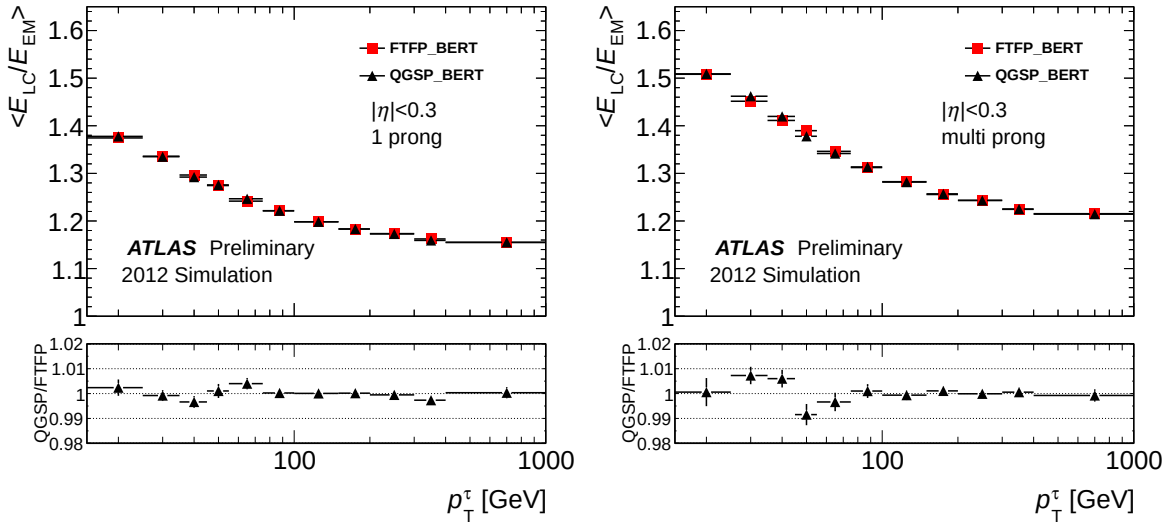

(a) (b)

Figure 6: Comparison of the effective LC calibration at the $\tau_{\text{had-vis}}$ level as given by $\langle E_{LC}/E_{EM}\rangle$ between two different shower models as a function of the transverse momentum of $\tau_{\text{had-vis}}$ for $\tau_{\text{1-prong}}$ (a) and $\tau_{\text{multi-prong}}$ (b). For $\tau_{\text{1-prong}}$, the dependence is smaller due to lower hadronic activity.

in E/p results at the EM scale to those obtained at the LC scale $(\text{Data/MC})_{EM}/(\text{Data/MC})_{LC}$. These comparisons show deviations smaller than 1%. Therefore an additional uncertainty of 1% for $\tau_{\text{multi-prong}}$ and 0.5% for $\tau_{\text{1-prong}}$ is assigned due to an imperfect shower model.

3.1.6 Calorimeter Response Results

For $|\eta^\tau| < 0.8$, the uncertainty from high momentum charged hadrons is derived from the CTB analysis. Figure 7 shows the TES bias (central value) and uncertainty (error bars) due to the calorimeter response with all contributions folded in. The error bars are the fitted width, while the points represent the expected scale bias between simulation and data. Overall, low momentum hadrons show a lower response in data than in simulation in the $\langle E/p\rangle$ analysis. This translates into an expected TES shift of the order of 1% for $p_T^\tau = 15$ GeV. The response uncertainty is of the order of 1.5-2% for $\tau_{\text{1-prong}}$ while it is about 2-2.5% for $\tau_{\text{multi-prong}}$. The expected scale shift is smaller than the uncertainty, hence no calibration correction is extracted. Instead, the expected shift is added in quadrature to the uncertainty.

Figure 8 shows the TES uncertainty derived from the $\langle E/p\rangle$ analysis and e/γ scale uncertainties for the $0.8 < |\eta^\tau| < 2.5$ region. Additional uncertainties for high momentum charged hadrons need to be folded in for a complete response uncertainty. The response uncertainty for high momentum charged hadrons is evaluated by comparing the nominal hadronic shower model to the FTFP_BERT shower model. These systematic uncertainties are provided in Table 2, as a function of p_T^τ, $|\eta^\tau|$ and n_p and need to be scaled by the energy fraction carried by particles outside the scope of the $\langle E/p\rangle$ measurement.

3.2 Additional Uncertainties on the TES Calibration

Additional uncertainties are evaluated from four distinct sources: knowledge of the dead material in front of the calorimeters, underlying event model, the non-closure of the calibration method and pileup [12].

An increase in dead material affects the energy deposition in the calorimeters, that is not accounted for in the calibration procedure. To quantify the systematic uncertainty due to our knowledge of the

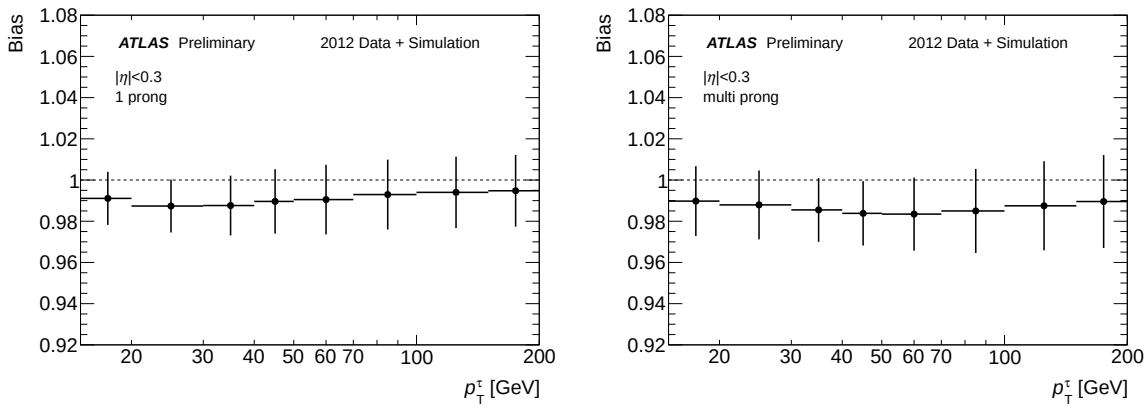

(a) $\tau_{\text{1-prong}}$

(b) $\tau_{\text{multi-prong}}$

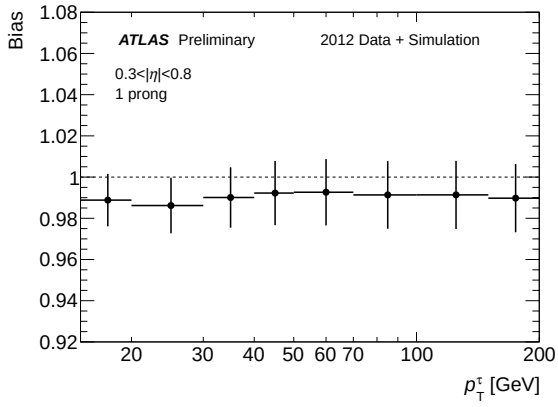

(c) $\tau_{\text{1-prong}}$

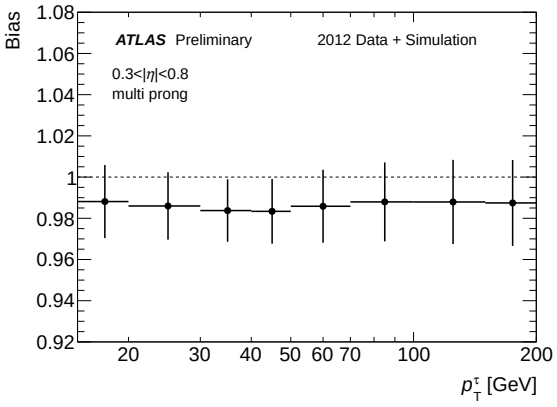

(d) $\tau_{\text{multi-prong}}$

Figure 7: Expected relative calorimeter response shift of the data with respect to the MC of reconstructed transverse momentum of the τ candidate in two pseudorapidity bins. The error bars represent the TES uncertainty due to calorimeter response uncertainties.

One-prong systematics	$0.8 < \lvert\eta^\tau\rvert < 1.3$	$1.3 < \lvert\eta^\tau\rvert < 1.6$	$\lvert\eta^\tau\rvert > 1.6$
> 15 GeV	0.5%	1.0%	0.5%
Multi-prong systematics	$0.8 < \lvert\eta^\tau\rvert < 1.3$	$1.3 < \lvert\eta^\tau\rvert < 1.6$	$\lvert\eta^\tau\rvert > 1.6$
15-30 GeV	2.0%	3.0%	1.0%
30-100 GeV	2.0%	2.0%	1.0%
> 100 GeV	1.0%	1.0%	0.5%

Table 2: Systematic uncertainty due to the shower model as a function of p_T^τ and $|\eta^\tau|$. The uncertainty is not scaled by the energy fraction carried by particles outside the scope of the $\langle E/p \rangle$ measurement.

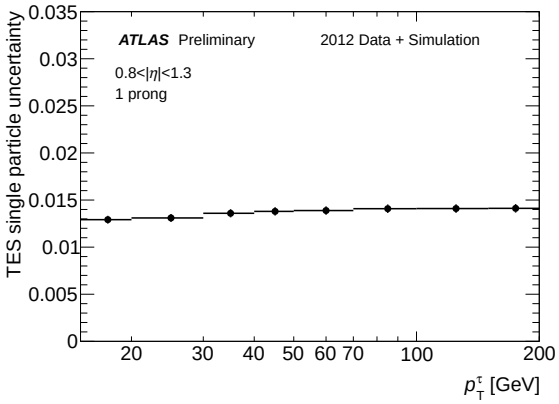

(a) $\tau_{\text{1-prong}}$

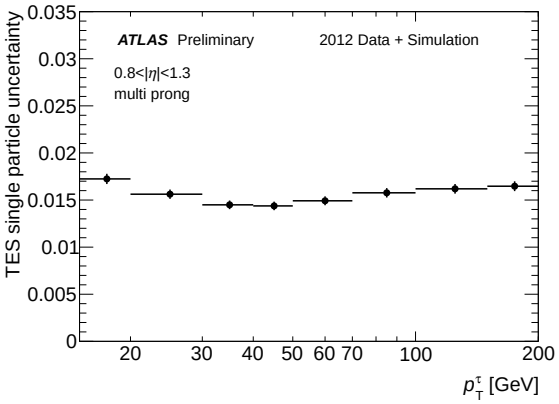

(b) $\tau_{\text{multi-prong}}$

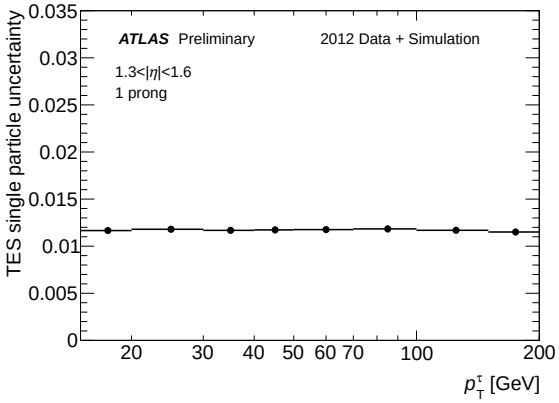

(c) $\tau_{\text{1-prong}}$

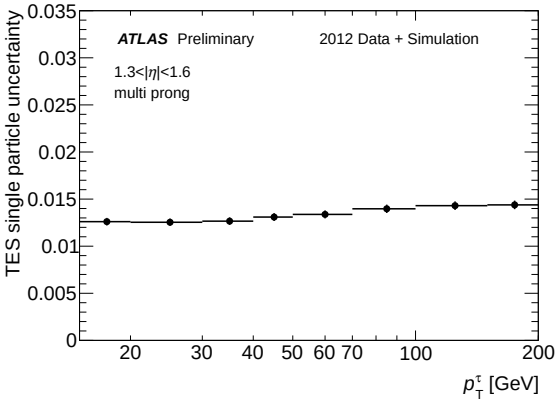

(d) $\tau_{\text{multi-prong}}$

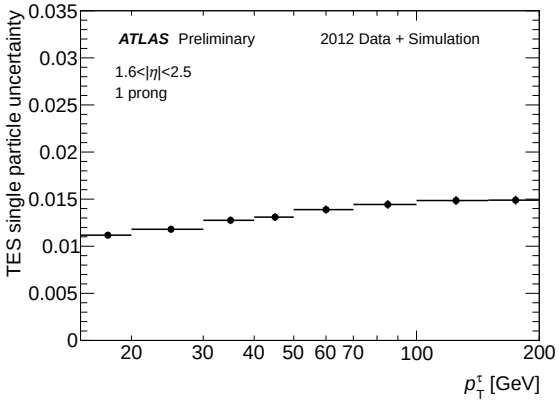

(e) $\tau_{\text{1-prong}}$

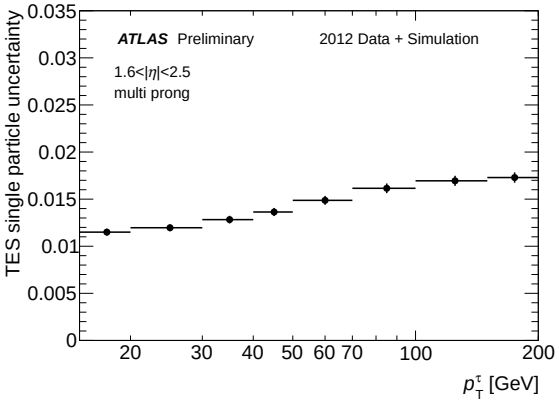

(f) $\tau_{\text{multi-prong}}$

Figure 8: Calorimeter response uncertainty for $0.8 < |\eta^\tau| < 2.5$ in three pseudorapidity bins, for $\tau_{\text{1-prong}}$ (left) and $\tau_{\text{multi-prong}}$ (right) . Only contributions from the $\langle E/p \rangle$ analysis and e/γ scale uncertainties are taken into account.

material in the ATLAS Inner Detector and the cryostat, the nominal sample is compared to a dataset generated with a conservative extra amount of material in the detector simulation [12]. The simulated dataset has an extra 5% material in the Inner Detector, distributed between its sub-detectors, and an extra 20% of material for detector services added for the Pixels. Between the Semiconductor Tracking Detector and Transition Radiation Tracker, there is an additional 20% of material for detector services included and 15% of extra material is added at the end of the Inner Detector end-plate. The dead material contribution to the TES uncertainty is scaled by the energy fraction carried by particles outside the $\langle E/p \rangle$ measurement, since this measurement is sensitive to the amount of dead material in front of the calorimeter. On average, the dead material knowledge contributes between 1% and 2% to the TES uncertainty.

The uncertainty due to the underlying event model is obtained by comparing the TES of the nominal sample with a dataset generated using a different MC tune for the underlying event [23]. On average, the underlying event model contributes about 1% to the TES uncertainty. The non-closure of the calibration method contributes about 1% to the TES uncertainty for $\tau_{\text{1-prong}}$ and 2% for $\tau_{\text{multi-prong}}$.

After applying the pileup correction (described in Section 2.3), the variation of the response as a function of N_{PV} is significantly reduced. The remaining dependence is assigned as a systematic uncertainty. It is estimated by splitting the MC samples into five bins according to the average number of primary vertices, which range from 0 to 40. This uncertainty is assigned independent of $|\eta^\tau|$. Figure 9 shows the ratio $(p_T^\tau - p_T^{\text{true}})/p_T^{\text{true}}$ as a function of $|\eta^\tau|$ and p_T^τ for different number of primary vertices. The difference between the highest and lowest value is taken as the pileup uncertainty to avoid double counting the systematics deriving from the non-closure. This uncertainty is found to be 3% for $15 < p_T^\tau < 20$ GeV and up to 2% for $p_T^\tau > 20$ GeV. To estimate the impact of possible out-of-time pileup contributions on the energy response, the scale dependence on the average number of interactions per bunch crossing ($\langle \mu \rangle$) at a fixed value of N_{PV} was studied and found to be negligible. Therefore no additional uncertainty is assigned.

A summary of the pileup uncertainties is provided in Table 3, as a function of p_T^τ and n_p. The uncertainties are independent of the chosen identification working point.

One-prong systematics		Multi-prong systematics	
15-20 GeV	3%	15-20 GeV	3%
20-30 GeV	2%	20-60 GeV	2%
30-80 GeV	1%	60-80 GeV	1%
> 80 GeV	0.5%	> 80 GeV	0.5%

Table 3: Systematic uncertainties due to the pileup correction in bins of p_T^τ. Bins in p_T^τ with equal uncertainties are grouped.

3.3 Total Systematic Error

Figure 10 and Table 4 summarise the TES systematic uncertainties for reconstructed τ_h candidates passing a medium particle identification criteria. Table 5 summarises the TES systematic uncertainties for reconstructed τ_h candidates passing a tight particle identification criteria [10].

The uncertainty is smallest for $\tau_{\text{1-prong}}$ in the central region. The transition region between barrel and end-cap ($1.3 < |\eta^\tau| < 1.6$) has the largest uncertainty, mainly due to the large amount of dead material in front of the calorimeter.

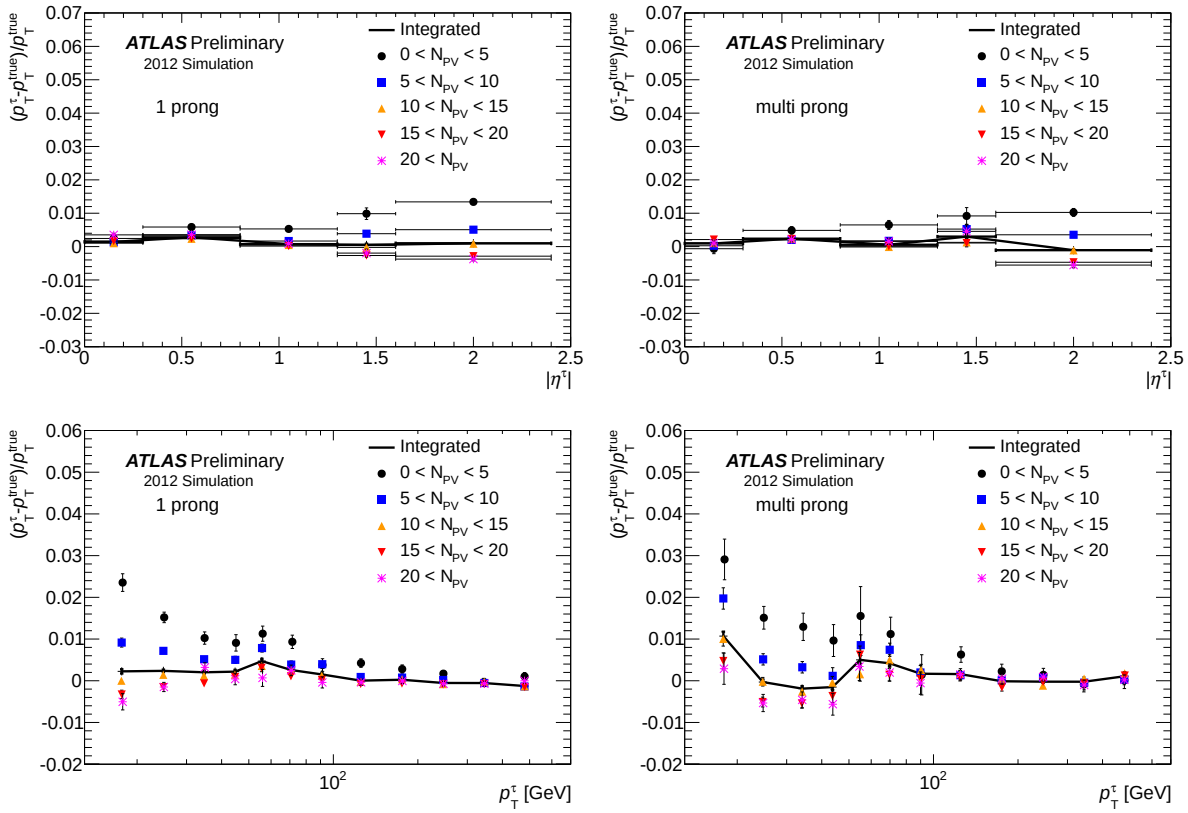

Figure 9: Response distributions after pileup correction as a function of $|\eta^\tau|$ (top) and p_T^τ (bottom) for different number of primary vertices. Shown are $\tau_{\text{1-prong}}$ (left) and $\tau_{\text{multi-prong}}$ (right).

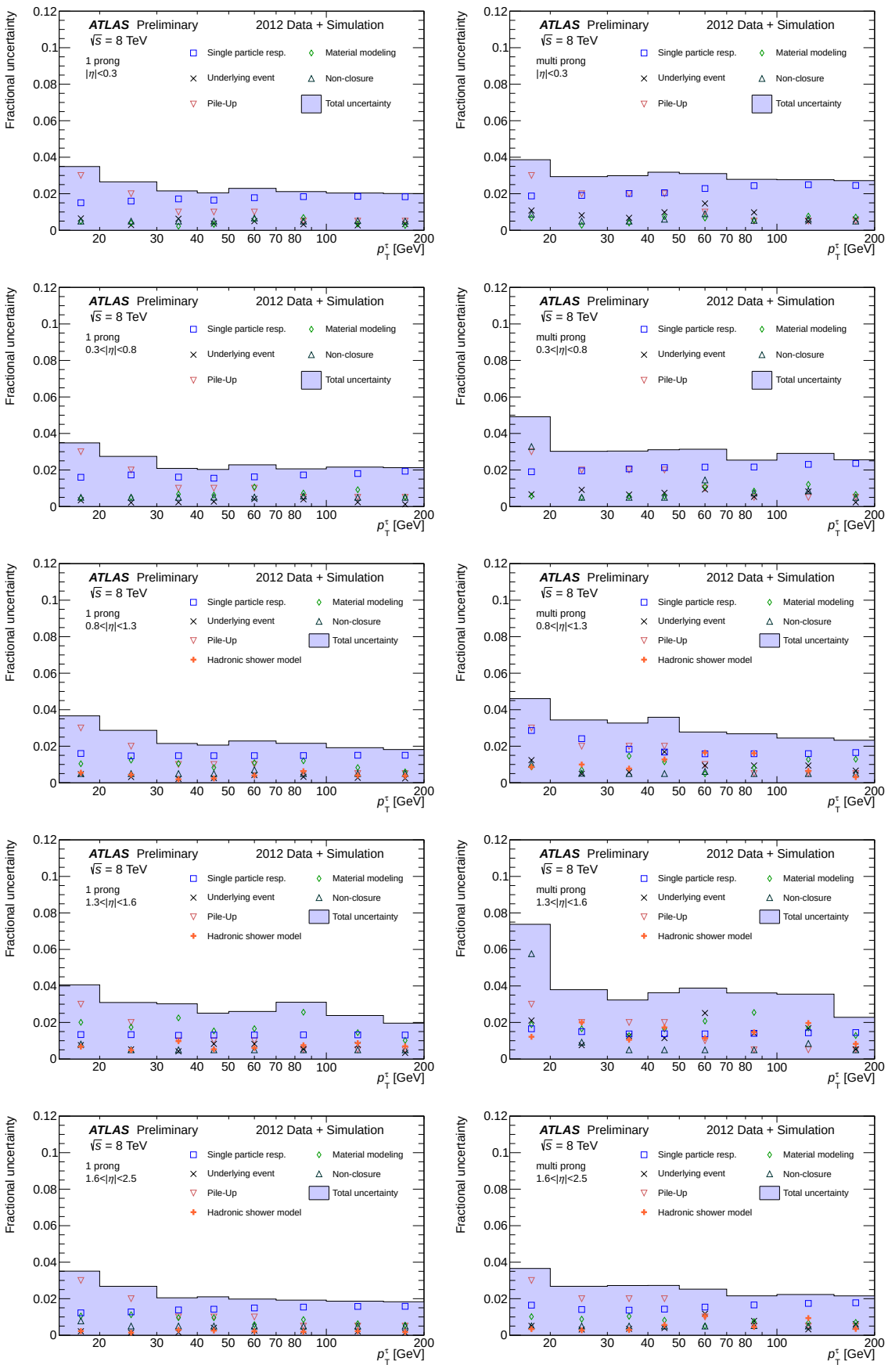

Figure 10: TES uncertainty for $\tau_{\text{1-prong}}$ (left) and $\tau_{\text{multi-prong}}$ (right) in various η^τ bins. The individual contributions are shown as points and the combined uncertainty is shown as a filled band. Bins in p_T^τ with equal uncertainties are grouped.

One-prong systematics	$\|\eta^\tau\| < 0.3$	$0.3 < \|\eta^\tau\| < 0.8$	$0.8 < \|\eta^\tau\| < 1.3$	$1.3 < \|\eta^\tau\| < 1.6$	$\|\eta^\tau\| > 1.6$
15-20 GeV	3.5%	3.5%	3.5%	4%	3.5%
20-30 GeV	2.5%	3%	3%	3%	2.5%
30-100 GeV	2%	2%	2%	3%	2%
100-150 GeV	2%	2%	2%	2.5%	2%
> 150 GeV	2%	2%	2%	2%	2%
Multi-prong systematics	$\|\eta^\tau\| < 0.3$	$0.3 < \|\eta^\tau\| < 0.8$	$0.8 < \|\eta^\tau\| < 1.3$	$1.3 < \|\eta^\tau\| < 1.6$	$\|\eta^\tau\| > 1.6$
15-20 GeV	4%	5%	4.5%	7.5%	3.5%
20-50 GeV	3%	3%	3.5%	4%	2.5%
50-70 GeV	3%	3%	2.5%	4%	2.5%
70-150 GeV	2.5%	2.5%	2.5%	3.5%	2%
> 150 GeV	2.5%	2.5%	2.5%	2.5%	2%

Table 4: Total systematic uncertainty as a function of the p_T^τ and $|\eta^\tau|$ for $\tau_{\text{1-prong}}$ and $\tau_{\text{multi-prong}}$ passing medium identification criteria.

4 Tau Energy Scale Uncertainty from $Z \to \tau\tau$ Events

The reconstructed visible mass peak of $Z \to \mu\nu_\mu\nu_\tau\tau_h\nu_\tau$ decays can be used to measure both the TES and its uncertainty in-situ. This method is used here to provide a cross check of the TES calibration. This is especially important in the region where no CTB data are available ($0.8 < |\eta| < 2.5$).

The visible mass ($\sqrt{\|p_\mu + p_{\tau_{\text{had-vis}}}\|^2}$) of $Z \to \mu\nu_\mu\nu_\tau\tau_h\nu_\tau$ decays is defined as invariant mass of the reconstructed momenta of the visible decay products. As the muon momentum scale is determined independently with high precision, this visible mass can be used to constrain the TES through its dependence on p_T^τ. The value of the TES can be found by shifting the fully reconstructed p_T^τ in the simulation and comparing the resulting visible mass peak to that observed in data. In this method, shifts of the TES are parametrised according to the following ansatz

$$p_T^{'\tau} = (1 + \alpha)p_T^\tau \tag{8}$$

where α is a parameter that accounts for the TES variation.

The MC samples used in this study are fully simulated. While $W(\to \tau\nu)$+jets, $Z \to \tau\tau$ and $\gamma/Z(\to \mu\mu)$+jets samples are generated using ALPGEN [24] and HERWIG [25] for the parton shower model, the $W(\to \mu\nu)$+jets sample is generated using POWHEG [26]+PYTHIA8 [9] and the $t\bar{t}$ sample is generated using MC@NLO [25] followed by a parton showering in HERWIG.

The results are based on proton-proton collision data collected at the LHC at $\sqrt{s} = 8$ TeV in early 2012. The integrated luminosity of the dataset after basic data quality criteria corresponds to 4.5 fb^{-1}.

4.1 Event Selection

Events are preselected using a single muon trigger which requires one well-isolated muon candidate with a transverse momentum of $p_T^\mu > 20$ GeV. Collision events that passed the trigger selection are further required to have a reconstructed primary vertex with at least four associated tracks. Quality criteria are applied to reject events that originate from non-collision backgrounds, cosmic ray background or calorimeter noise [27]. Events are then selected if they contain exactly one isolated muon and at least one τ_h of opposite sign. Muons are reconstructed by matching tracks in the muon spectrometer with tracks in the Inner Detector [28]. Candidates are required to have $|\eta^\mu| < 2.4$ and $p_T^\mu > 22$ GeV, to ensure that they are in the plateau of the trigger efficiency curve. The candidate's track is further required to

One-prong systematics	$\lvert\eta^\tau\rvert < 0.3$	$0.3 < \lvert\eta^\tau\rvert < 0.8$	$0.8 < \lvert\eta^\tau\rvert < 1.3$	$1.3 < \lvert\eta^\tau\rvert < 1.6$	$\lvert\eta^\tau\rvert > 1.6$
15-20 GeV	4%	4%	4%	4%	3.5%
20-30 GeV	3%	3%	3%	4%	3%
30-100 GeV	2.5%	2.5%	2.5%	3%	2%
100-150 GeV	2%	2.5%	2%	3%	2%
> 150 GeV	2%	2.5%	2%	2%	2%
Multi-prong systematics	$\lvert\eta^\tau\rvert < 0.3$	$0.3 < \lvert\eta^\tau\rvert < 0.8$	$0.8 < \lvert\eta^\tau\rvert < 1.3$	$1.3 < \lvert\eta^\tau\rvert < 1.6$	$\lvert\eta^\tau\rvert > 1.6$
15-20 GeV	4.5%	4%	5.5%	6%	3.5%
20-30 GeV	4%	3.5%	4.0%	4%	3%
30-50 GeV	3.5%	3.5%	3.5%	4%	3%
50-70 GeV	3%	3.5%	3.5 %	4%	3%
70-150 GeV	3%	3%	3%	4%	2.5%
> 150 GeV	3%	3%	2.5%	3.5%	2.5%

Table 5: Total systematic uncertainty as a function of the p_T^τ and $|\eta^\tau|$ for $\tau_{\text{1-prong}}$ and $\tau_{\text{multi-prong}}$ passing tight identification criteria.

have a minimum distance from the primary vertex in the z direction of less than 10 mm to satisfy track quality criteria.

The degree of isolation of the muon is the strongest discriminator against QCD multi-jet events. Calorimeter isolation is imposed by requiring the energy deposited in the EM and hadronic calorimeters which is not associated to the muon in a cone of $\Delta R = 0.2$ to be less than 4% of p_T^μ. Furthermore, track isolation is imposed by requiring that there are no additional tracks with $p > 1$ GeV associated to the muon within $\Delta R < 0.4$.

Hadronic τ candidates are required to have $p_T^\tau > 20$ GeV and $|\eta^\tau| < 2.5$. To reduce contamination from jets, τ_h candidates are required to have one or three associated tracks, unit charge and to pass medium identification criteria [10]. In case more than one τ_h is reconstructed, the candidate with the highest p_T^τ is selected. Events with electrons are vetoed, as well as events where the τ_h is found to be consistent with being an electron or muon [29]. Additionally, τ_h candidates matching reconstructed muons with an Inner Detector track and a segmented track in the muon spectrometer within $\Delta R < 0.2$ are rejected.

The $W(\rightarrow \mu\nu)$+jets background is reduced by using the following selection criteria

$$\cos\Delta\phi(\tau_{\text{had-vis}}, E_{\text{T}}^{\text{miss}}) + \cos\Delta\phi(\mu, E_{\text{T}}^{\text{miss}}) > -0.15 \tag{9}$$

$$m_T = \sqrt{2p_T^\mu \cdot E_{\text{T}}^{\text{miss}}(1 - \cos\Delta\phi(\mu, E_{\text{T}}^{\text{miss}}))} < 50 \text{ GeV} \tag{10}$$

where $E_{\text{T}}^{\text{miss}}$ is the missing transverse momentum, which is reconstructed from energy deposited in calorimeter cells and muons reconstructed in the muon spectrometer [30].

4.2 Background Estimation

The background contributions from $Z(\rightarrow \mu\mu)$+jets and $t\bar{t}$ processes are small and estimated from simulated events. The $W(\rightarrow \mu\nu)$+jets and the multi-jet background estimations are described below. A potential contribution from Higgs boson events is expected to be smaller than 0.4% of the $Z \rightarrow \tau\tau$ contribution and is neglected.

4.2.1 W + Jet(s) Background

The $W(\rightarrow \mu\nu)$+jets and $W(\rightarrow \tau\nu)$+jets processes contaminate the selected sample when a jet mimics the τ_h signature. The rate of these mis-identified events is not well modelled in the simulation [31], thus the prediction from simulation is normalised using scale factors derived from data.

The scale factors are measured in a W+jets control region separately for $|\eta^\tau| < 0.8$ and $0.8 < |\eta^\tau| < 2.5$, and applied to the W+jets background in the signal region. This W-enriched control region is obtained by reversing the W+jets suppression criteria given in equations 9 and 10. The scale factors k_W are then obtained by dividing the number of events in data, after subtracting the small non-W MC estimated background, by the number of W events predicted by the simulation. The k_W factors are found to be 0.915 ± 0.016 (stat.) for the region $|\eta^\tau| < 0.8$ and 0.867 ± 0.013 (stat.) for the region $0.8 < |\eta^\tau| < 2.5$.

4.2.2 Multi-jet Background

The background due to multi-jet events is estimated using a data driven method. A multi-jet enriched control region is constructed by requiring the τ_h candidate and the muon candidate to have same sign charge (SS). The ratio of events where the charge of the decay products have the opposite sign to those where they have the same sign, $R_{OS/SS}$, is then measured in a separate pair of control regions where the lepton isolation requirement is inverted. Electroweak and $t\bar{t}$ backgrounds in all control regions are subtracted using simulated events. The shape of the visible mass distribution is taken from the SS, lepton isolated region and scaled with the normalisation factor $R_{OS/SS}$. This estimation is performed in each η^τ region separately. The normalisation factors are found to be 1.177 ± 0.026 (stat.) for $|\eta^\tau| < 0.8$ and 1.086 ± 0.019 (stat.) for $0.8 < |\eta^\tau| < 2.5$.

4.3 TES Estimation

The observed visible mass distribution is matched to a range of templates to derive the value of α which best describes the data. These templates are generated using the simulated samples for the signal, electroweak and $t\bar{t}$ background, and data for the multi-jet background. For each simulated sample, α is varied between -10% and 5% in 0.2% steps. The median of the visible mass distribution is used to select the template which best describes the data, as it is found to be more stable with respect to statistical fluctuations than other methods. Figure 11 shows a selection of the templates, with data superimposed, for the two η^τ regions considered. Table 6 shows the value of α obtained for these $|\eta^\tau|$ regions. Here α can be interpreted as the percentage scale to be applied to the TES such that the simulation matches the data. The difference in the α values extracted in $|\eta^\tau| < 0.8$ and $0.8 < |\eta^\tau| < 2.5$ is found to be 1.4%.

region	preferred α value	difference
$\lvert\eta^\tau\rvert < 0.8$	-3%	-
$0.8 < \lvert\eta^\tau\rvert < 2.5$	-1.6%	1.4%

Table 6: α values for the data visible mass distributions for the different η regions.

To propagate the statistical uncertainty from the data, each bin of the observed visible mass distributions is varied within its statistical uncertainty and the modified sample is used to determine the scale shift. This is repeated for 1000 toy experiments and the standard deviation of the resulting distribution of α values is taken as statistical uncertainty on the nominal value. This leads to an uncertainty of 0.9% for all $|\eta^\tau|$ regions. The uncertainty due to the limited statistics in the simulated distributions used to generate the template, from now on referred to as *the model*, is evaluated in a similar way and found to be 1.3% for $|\eta^\tau| < 0.8$ and 0.9% for $0.8 < |\eta^\tau| < 2.5$.

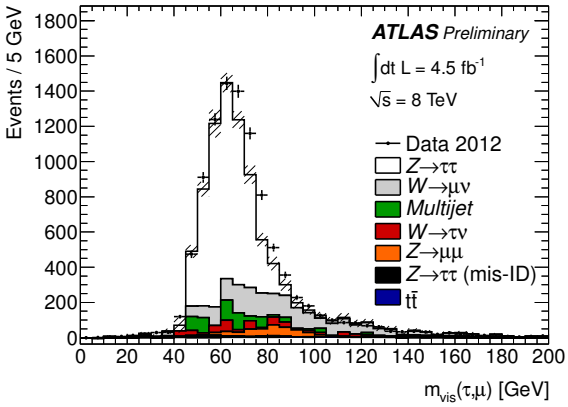

(a) $|\eta^{\tau}| < 0.8$, $\alpha = -10\%$

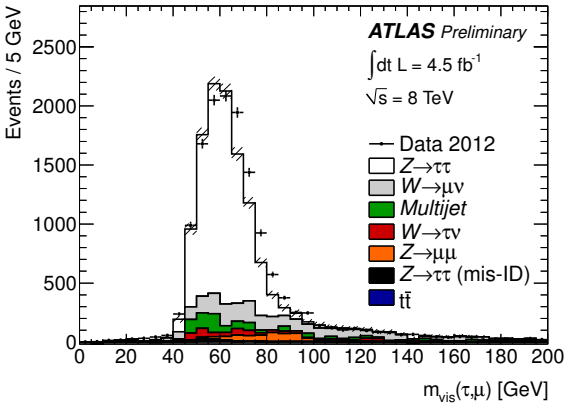

(b) $0.8 < |\eta^{\tau}| < 2.5$, $\alpha = -10\%$

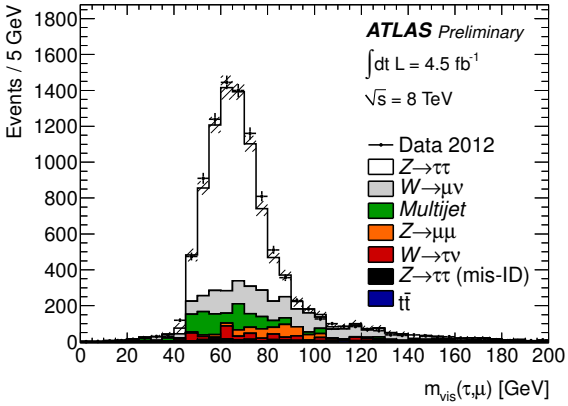

(c) $|\eta^{\tau}| < 0.8$, $\alpha = -3.0\%$

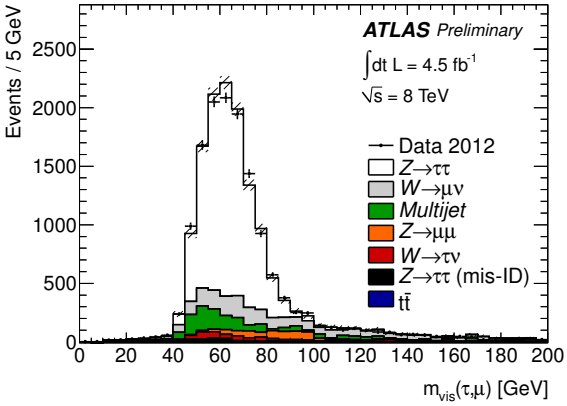

(d) $0.8 < |\eta^{\tau}| < 2.5$, $\alpha = -1.6\%$

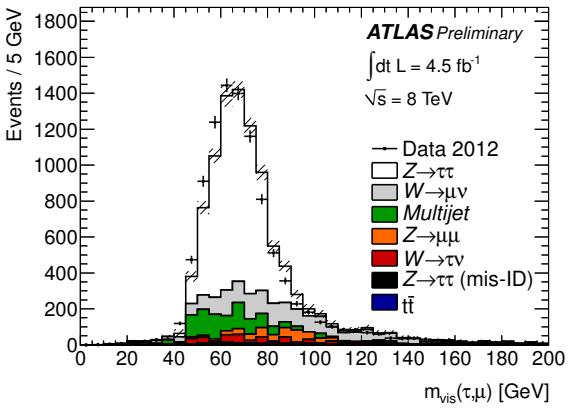

(e) $|\eta^{\tau}| < 0.8$, $\alpha = +5\%$

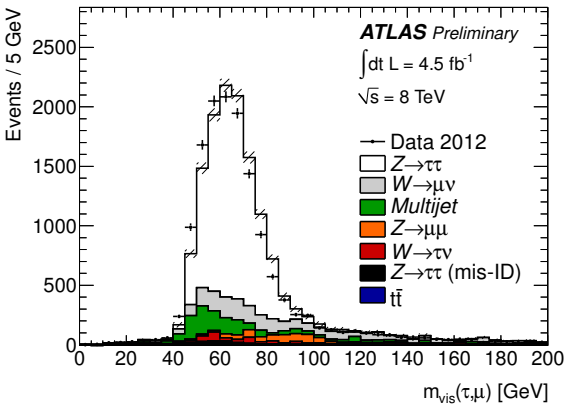

(f) $0.8 < |\eta^{\tau}| < 2.5$, $\alpha = +5\%$

Figure 11: Templates for $|\eta^{\tau}| < 0.8$ and $0.8 < |\eta^{\tau}| < 2.5$ for values for α of -10% (a,b), +5% (e,f) and the best match with the data (c,d).

4.4 Systematic Uncertainties

The dominant systematic uncertainties are arising from:

- Tau and muon identification efficiency.
- Muon transverse momentum resolution.
- Energy scale and resolution of the soft component of missing transverse momentum.
- The W + jets and multi-jet background estimates.
- MC generator uncertainty.

Each of these uncertainties is evaluated by generating new templates and repeating the scale determination with these systematically varied samples. The resulting systematic uncertainty on the scale estimate due to the measured τ_h identification scale factor is ± 2.4%. Systematic uncertainties due to muon identification scale factors and transverse momentum resolution are both of order ± 1%, whereas the systematic uncertainties due to scale and resolution of the soft $E_{\mathrm{T}}^{\mathrm{miss}}$ term are of order ± 3%. To estimate the uncertainty due to the $W(\rightarrow \mu\nu)$+jets shape models, the analysis was repeated using a $W(\rightarrow \mu\nu)$+jets sample generated with ALPGEN and the difference is conservatively assigned as a systematic uncertainty.

As the analysis is used to constrain the scale differences between $|\eta| < 0.8$ and $0.8 < |\eta| < 2.5$, most of these systematic effects cancel in the difference of the preferred values of α. These uncertainties are summarised in Table 7. The total uncertainty is obtained by summing in quadrature the statistical and systematic uncertainties in both regions is found to be 3.6%.

	Source of uncertainty	Uncertainty
Statistical	Data	1.3%
	Model	1.6%
Systematic	Muon p_T resolution (Inner Detector)	1.6%
	Muon p_T resolution (μ Spectrometer)	1.4%
	Muon ID efficiency scale factor	$< \pm 0.2\%$
	Tau ID efficiency scale factor	0.4%
	Soft $E_{\mathrm{T}}^{\mathrm{miss}}$ term resolution	0.4%
	Soft $E_{\mathrm{T}}^{\mathrm{miss}}$ term scale	0.4%
	W + jets scale factor	0.4%
	$W(\rightarrow \mu\nu)$+jets generator uncertainty	1.8%
Total		3.6%

Table 7: Summary of the uncertainties on the difference in the preferred α values from $|\eta^\tau| < 0.8$ to $0.8 < |\eta^\tau| < 2.5$

4.5 Results

The aim of this analysis is to use $Z \rightarrow \tau\tau$ events to cross-check the procedure used to assess the TES systematic uncertainty for the $0.8 < |\eta^\tau| < 2.5$ region, where no CTB data was available to constrain the

hadron response uncertainty. This cross check is performed by estimating the difference in the α values extracted in $|\eta^\tau| < 0.8$ and $0.8 < |\eta^\tau| < 2.5$, where α is the scale to be applied to the TES so that the simulation matches data. This difference is found to be $(1.4 \pm 3.6)\%$, which is consistent with zero within the uncertainty. Furthermore the obtained uncertainties are of the same order of magnitude as the ones obtained in Section 3.3. A comparison of different shower models was used in Section 3.1.6 to replace the missing information from CTB data at pseudorapidities $0.8 < |\eta^\tau| < 2.5$ for high momentum particles. This simple comparison of different simulated samples cannot yield any information about possible scale shifts between data and simulated samples. A fully data driven estimate of the uncertainty was given for ($|\eta| < 0.8$). Since no significant scale shift between the two pseudorapidity regions is observed in this data driven study, the absence of CTB calibrations beyond $|\eta^\tau| = 0.8$ does not lead to increased uncertainties at larger $|\eta^\tau|$. The simulated samples seem to describe the scale dependence on $|\eta^\tau|$ sufficiently well. A possible scale shift is shown to be smaller than the assigned systematic uncertainties.

5 Conclusions

This note describes the energy calibration for hadronic τ decays, as well as two independent methods to determine the systematic uncertainties on this energy scale, for data collected in 2012 at 8 TeV centre-of-mass energy. Because hadronic τ decays consist of a specific mix of charged and neutral pions, the energy scale of τ_h candidates is derived independently of the jet energy scale. The systematic uncertainty on the TES is calculated using the convolution of individual visible τ_h decay products, namely charged and neutral pions.

The systematic uncertainty on the calorimeter response is given by a mixture of in-situ $\langle E/p \rangle$ and CTB measurements for $|\eta^\tau| < 0.8$ and a combination of in-situ $\langle E/p \rangle$ measurements and MC simulation for $0.8 < |\eta^\tau| < 2.5$. Using this procedure, the final systematic uncertainty for $p_T^\tau > 20$ GeV is found to be $\leq 3\%$ for $\tau_{\text{1-prong}}$, and $\leq 4\%$ for $\tau_{\text{multi-prong}}$, over the full pseudorapidity range for τ decays passing medium identification cuts. The largest uncertainty is found to be for $15 < p_T^\tau < 20$ GeV and $1.3 < |\eta^\tau| < 1.6$, where it increases to a maximum of 4% for $\tau_{\text{1-prong}}$ and 7.5% for $\tau_{\text{multi-prong}}$.

The systematic uncertainty quoted using the deconvolution method in the region where no CTB data were available ($0.8 < |\eta^\tau| < 2.5$) is cross-checked with $Z \to \tau\tau$ events in a dataset of 4.5fb^{-1}. The reconstructed visible mass peak of $Z \to \tau\tau$ is used to derive a correction to be applied to the TES such that the simulation matches the data. This scale is calculated independently in both $|\eta^\tau| < 0.8$ and $0.8 < |\eta^\tau| < 2.5$ regions. This cross-check finds that the scale difference between the two regions is consistent with zero within the error, thus confirming the systematic uncertainty assigned by the deconvolution method in the region $0.8 < |\eta^\tau| < 2.5$.

References

[1] ATLAS Collaboration, *Search for the Standard Model Higgs boson in $H \to \tau^+\tau^-$ decays in proton-proton collisions with the ATLAS detector*, ATLAS-CONF-2012-160, http://cds.cern.ch/record/1493624.

[2] ATLAS Collaboration, *Search for Supersymmetry in Events with Large Missing Transverse Momentum, Jets, and at Least One Tau Lepton in 7 TeV Proton-Proton Collision Data with the ATLAS Detector*, Eur. Phys. J. **C72** (2012) 2215, arXiv:1210.1314 [hep-ex].

[3] J. Beringer, et al., *Particle Data Group*, Phys. Rev. **D86** (2012) 010001.

[4] ATLAS Collaboration, *Determination of the tau energy scale and the associated systematic uncertainty in proton-proton collisions at sqrts = 7 TeV with the ATLAS detector at the LHC in 2011*, ATLAS-CONF-2012-054, http://cdsweb.cern.ch/record/1453781.

[5] M. Cacciari, G. P. Salam, and G. Soyez, *The Anti-k(t) jet clustering algorithm*, JHEP **0804** (2008) 063.

[6] W. Lampl, et al., *Calorimeter Clustering Algorithms: Description and Performance*, ATL-LARG-PUB-2008-002, http://cds.cern.ch/record/1099735.

[7] T. Barillari, et al., *Local Hadronic Calibration*, ATL-LARG-PUB-2009-001-2, http://cds.cern.ch/record/1112035.

[8] S. Agostinelli, et al., *GEANT4: A simulation toolkit*, Nucl. Instr. and Meth. **A506** (2003) 250.

[9] T. Sjostrand, S. Mrenna, and P. Z. Skands, *PYTHIA 6.4 Physics and Manual*, JHEP **0605** (2006) 26.

[10] ATLAS Collaboration, *Performance of the Reconstruction and Identification of Hadronic Tau Decays in ATLAS with 2011 Data*, ATLAS-CONF-2012-142, http://cdsweb.cern.ch/record/1485531.

[11] E. Khramov et al., *Study of the Response of the Hadronic Barrel Calorimeter in the ATLAS Combined Test-beam to Pions of Energies from 20 to 350 GeV for Beam Impact Points from 0.2 to 0.65*, ATL-TILECAL-PUB-2009-007, http://cds.cern.ch/record/1172156.

[12] ATLAS Collaboration, *Reconstruction, Energy Calibration, and Identification of Hadronically Decaying Tau Leptons*, ATLAS-CONF-2011-077, http://cdsweb.cern.ch/record/1353226.

[13] ATLAS Collaboration, *ATLAS Calorimeter Response to Single Isolated Hadrons and Estimation of the Calorimeter Jet Scale Uncertainty*, ATLAS-CONF-2011-028, http://cdsweb.cern.ch/record/1337075.

[14] ATLAS Collaboration, *ATLAS Calorimeter Response to Single Isolated Hadrons and Estimation of the Calorimeter Jet Scale Uncertainty*, ATLAS-CONF-2010-052, http://cds.cern.ch/record/1281309.

[15] ATLAS Collaboration, *Jet energy scale and its systematic uncertainty in proton-proton collisions at sqrt(s)=7 TeV in ATLAS 2010 data*, ATLAS-CONF-2011-032, http://cdsweb.cern.ch/record/1337782.

[16] ATLAS Collaboration, *The ATLAS Simulation Infrastructure*, Eur. Phys. J. **C70** (2010) 823.

[17] ATLAS Collaboration, *Electron performance measurements with the ATLAS detector using the 2010 LHC proton-proton collision data*, Eur. Phys. J. **C72** (2012) 001.

[18] ATLAS Collaboration, *Response of the ATLAS calorimeters to single isolated hadrons produced in proton proton collisions at a center of mass energy of sqrts = 900 GeV*, ATLAS-CONF-2010-017, http://cdsweb.cern.ch/record/1277648.

[19] G. Folger and J. Wellisch, *String parton models in GEANT4*, in *Computing in High Energy and Nuclear Physics, CHEP, La Jolla, 2003*, eConf C0303241 MOMT007 (2003). arXiv:nucl-th/0306007.

[20] H. Bertini, *Intranuclear-cascade calculation of the secondary nucleon spectra from nucleon-nucleus interactions in the energy range 340 to 2900 MeV and comparisons with experiment*, Phys. Rev. **188** (1969) 1711–1730.

[21] M. Blann, B. Berman, and T. Komoto, *Precompound Model Analysis of Photonuclear Reactions*, Phys. Rev. **C28** (1983) 2286–2298.

[22] B. Andersson, G. Gustafson, and B. Nilsson-Almqvist, *A Model for Low p(t) Hadronic Reactions, with Generalizations to Hadron-Nucleus and Nucleus-Nucleus Collisions*, Nucl. Phys. **B281** (1987) 289.

[23] P. Z. Skands, *Tuning Monte Carlo Generators: The Perugia Tunes*, Phys. Rev. **D82** (2010) 074018.

[24] M. L. Mangano et al., *ALPGEN, a generator for hard multiparton processes in hadronic collisions*, JHEP **0307** (2003) 001.

[25] S. Frixione and B. Webber, *Matching NLO QCD computations and parton shower simulations*, JHEP **0206** (2002) 029.

[26] P. N. Frixione and C. Oleari, *Matching NLO QCD computations with Parton Shower simulations: the POWHEG method*, JHEP **0711** (2007) 070.

[27] ATLAS Collaboration, *Data-Quality Requirements and Event Cleaning for Jets and Missing Transverse Energy Reconstruction with the ATLAS Detector in Proton-Proton Collisions at a Center-of-Mass Energy of* $\sqrt{s}$ = 7 *TeV*, ATLAS-CONF-2010-038, http://cdsweb.cern.ch/record/1277678.

[28] ATLAS Collaboration, *Expected Performance of the ATLAS Experiment - Detector, Trigger and Physics*, arXiv:0901.0512 [hep-ex].

[29] ATLAS Collaboration, *Performance of the Reconstruction and Identification of Hadronic Tau Decays with ATLAS*, ATLAS-CONF-2011-152, http://cdsweb.cern.ch/record/1398195.

[30] ATLAS Collaboration, *Performance of Missing Transverse Momentum Reconstruction in Proton-Proton Collisions at 7 TeV with ATLAS*, Eur. Phys. J. **C72** (2012) 1844.

[31] ATLAS Collaboration, *Measurement of the Mis-identification Probability of Tau Leptons from Hadronic Jets and from Electrons*, ATLAS-CONF-2011-113, http://cdsweb.cern.ch/record/1375550.